Journal of Advanced Marine Engineering and Technology, Vol. 47, No. 4, pp. 195~201, 2023
J. Advanced Marine Engineering and Technology (JAMET)
https://doi.org/10.5916/jamet.2023.47.4.195

ISSN 2234-7925 (Print)
ISSN 2765-4796 (Online)
Original Paper

Effect of grain size on residual stress in $AlSi_{10}MnMg$ alloy

Minjeong Jeon[1] · Eunkyung Lee[†]

(Received August 23, 2023 ; Revised August 29, 2023 ; Accepted August 29, 2023)

Abstract: The effect of varying the grain size on the residual stress in $AlSi_{10}MnMg$ alloys prepared at various cooling rates was examined. The specimens with different initial grain sizes were manufactured by high-pressure die casting (HPDC) and gravity die casting (GDC) under heat treatment at 500 °C for 2 h, followed by furnace cooling and water quenching to control the variables that could affect the residual stress or induce microstructural changes. The average grain size of the non-heat-treated as-cast HPDC specimen was approximately 30 times smaller than that of the as-cast GDC specimen, and the residual stress of the large-grain GDC specimen was approximately 20 MPa larger. The grain size of the furnace-cooled GDC specimen was approximately 50 times larger than the average grain size of the furnace-cooled HPDC specimen, and the largest difference in the residual stress was approximately 40 MPa. The average grain sizes of the water-quenched GDC and HPDC specimens differed by approximately ten-fold, where the residual stress in the water-quenched GDC specimen was approximately 8 MPa higher. The larger the grain size, the more easily the low-angle grain boundaries are penetrated by the potential. Therefore, a larger the grain size leads to better distribution of the low-angle grain systems; thus, numerous dislocations were distributed inside and around the grain. The grain boundaries and dislocations that were highly aggregated inside the grain influenced the residual stress.

Keywords: High-pressure die casting (HPDC), Gravity die casting (GDC), Aluminum alloy, Residual stress, Grain size

1. Introduction

In recent years, the automobile industry has replaced most parts of conventional casting products with aluminum casting products to reduce the vehicle weight and improve the fuel efficiency. Cast iron and steel are conventionally the most widely used materials in the automotive industry; however, the use of aluminum alloy components instead of steel and cast iron is increasing **[1]**. Aluminum alloys constitute approximately one-third of steel materials and are recognized as representative lightweight materials that can replace steel materials and are used in engine-related parts such as the body, tire wheels, cylinder heads, and cylinder blocks **[2]**.

However, solidification and cooling during the casting process inevitably result in an uneven temperature distribution within the product, resulting in residual stress due to differences in the solidification rates of the molten materials during the aluminum casting process **[3]-[4]**. The residual stress of a casting part is the stress remaining in the casting after it has been removed from the mold. Castings typically contain large residual stresses due to the large heat gradients that are formed during the manufacturing process **[5]**.

Residual stresses resulting from uneven expansion and contraction within castings degrade the mechanical properties of parts, such as the fatigue life, dimensional stability, and breaking strength, and cause unexpected destruction during casting **[6]-[7]**.

When a product with a complex shape, such as a cylindrical head, is manufactured using a casting process, residual stress is generated because the rate and time of solidification vary from part to part **[8]**. Residual stress from castings leads to performance degradation, deformation, or cracking, which negatively affect the vehicle safety by reducing the durability **[9]-[10]**.

Residual stress is a defect that cannot be ignored in aluminum castings. Controlling residual stress is essential for the production of high-quality castings. Failure of the finished product due to unexpected destruction of the part is closely related to safety; therefore, predicting and understanding residual stress are

† Corresponding Author (ORCID: https://orcid.org/0000-0003-0723-8524): Associate Professor, Interdisciplinary Major of Maritime AI convergence, Department of Ocean Advanced Materials Convergence Engineering, Korea Maritime & Ocean University, 727, Taejong-ro, Yeongdo-gu, Busan 49112, Korea, E-mail: elee@kmou.ac.kr, Tel: 051-410-4353

1 M. S., Interdisciplinary Major of Maritime AI convergence, Department of Ocean Advanced Materials Convergence Engineering, Korea Maritime & Ocean University, E-mail: minjeong_eee@naver.com, Tel: 051-410-4955

important for quality assurance. Additional thermal treatment is required to remove the residual stress generated during the casting process. If the residual stress is not adequately relieved, deformation and cracks may occur, thereby reducing the durability of cast parts **[11]**.

In general, residual stress simulations predict the stress distribution based on changes in the convective heat transfer coefficient, elasticity coefficient, and yield strength depending on the heat transfer conditions, such as heating and cooling **[12]**. These simulations only predict the overall partial distortion on a macroscopic scale and cannot explain the stress on a microscopic scale **[13]**. Simulation systems for residual stress prediction do not consider the various characteristics of aluminum alloys, such as their microstructure and chemical properties; thus, the accuracy of the prediction is very poor. During the casting process, aluminum undergoes a large microstructural change before and after solidification; therefore, there is a large gap between the residual stress predicted by the simulation software and the empirically determined residual stress. Residual stress in aluminum castings is a defect that cannot be ignored. Despite the need for controlling residual stress to produce high-quality castings, studies on the residual stress and mechanism in aluminum castings remain insufficient to date. There are studies on the difference in the coefficient of thermal expansion of the base material versus the intermetallic compounds, and the effect of the growth of intermetallic compounds on residual stress; however, studies on the effect of grains, which are commonly observed in the microstructure, are insufficient **[14]-[15]**. Therefore, the development of a residual stress database by analyzing the effect of the grain size (which changes with heating and contraction during the casting process) on the development of residual stress is required.

Herein, the variables that affect the residual stress and microstructural changes in $AlSi_{10}MnMg$ alloy specimens manufactured by high-pressure die casting (HPDC) and gravity die casting (GDC) prepared through furnace cooling and water quenching heat treatment at 500 °C for 2 h are evaluated. This study aims to determine the optimal calibration conditions in order to improve the accuracy of residual stress prediction simulations by analyzing the effect of the grain size (which changes with the cooling rate) on the residual stress.

2. Experimental procedure

2.1 Materials

An $AlSi_{10}MnMg$ alloy with the composition listed in **Table 1** was used in this experiment. The $AlSi_{10}MnMg$ alloy is called AA365. AA365 is widely used in automobile part manufacturing owing to its excellent casting properties and good mechanical strength **[16]**. The specimens were manufactured using two casting methods: high-pressure die casting (HPDC) and gravity die casting (GDC). Compared with other casting methods, HPDC has many advantages, such as providing a fine-grain microstructure and good mechanical properties, because of its fast cooling speed **[17]**. Therefore, specimens with different initial grain sizes were produced using two different casting methods. Gravity die casting was conducted at 750 °C. AA365 ingots were melted in a graphite crucible furnace at 750 °C to obtain molten aluminum and injected into the mold. The manufactured specimens were heat treated at 500 °C for 2 h in an electronic furnace and then subjected to water quenching and furnace cooling. As mentioned, to vary the initial grain size, specimens were prepared using HPDC and GDC.

2.2 Microstructure analysis

The specimens of HPDC AA365 and GDC AA365 were polished with 200- to 2400-grit silicon carbide papers with a 0.25 μm diamond suspension and 0.04 μm colloidal suspension. In the finishing polishing step, the samples were ground with colloidal silica (CS) suspension (0.04−0.05 μm) for more than 20 min. In the final finishing step, water containing a surfactant was sprayed onto the sample for 60 s to remove the CS suspension adsorbed on the specimen surface. The microstructures of all specimens were observed using an optical microscope (OM; Eclipse LV150N, Nikon Metrology Inc.) and field-emission scanning electron microscopy (CLARA, Tescan) with electron backscatter diffraction (EBSD). EBSD data were collected with a step size of 2 μm using a field-emission scanning electron microscope with an acceleration voltage of 20 kV and beam current of ~9 nA. The raw EBSD data were processed using ATEX software.

2.3 Experimental evaluation of the residual stress

To quantitatively measure the residual stress, the sin 2ψ

Table 1: The composition of $AlSi_{10}MnMg$ aluminum alloy (wt.%)

	Si	Mn	Mg	Fe	Ti	Al
$AlSi_{10}MnMg$	10.6	≤0.7	≤0.29	0.11	≤0.08	Balance

method using X-ray diffraction (XRD) was used in this study. Because XRD can be used to accurately measure the residual stress in a non-destructive manner, the residual stress was measured using a literature method **[18]**. This method is based on Bragg's law using the sin2 ψ XRD method of analysis **[19]**.

XRD data were acquired at twelve different angles to increase the precision of the measurement; the residual stress was measured from the slope of the plot of sin2 ψ. CuKα X-rays (wavelength = 1.5405 Å) were used for XRD analysis of the Al material. The change in the diffraction peaks was observed in the 2θ range of 135–140° considering the appearance of a diffraction peak of the aluminum (422) surface at 137.5°.

3. Results and discussion

3.1 Microstructure

The secondary dendrite arm spacing (SDAS) was determined using **Equation (1)**. The entire length of the primary dendrite arm was measured as *L*, and the number of secondary arms *N* was counted along one side of the primary arm **[20]**.

$$\text{SDAS} = \frac{L}{N-1} \quad (1)$$

As shown in **Table 2**, the average SDAS value of the as-cast HPDC, furnace-cooled HPDC, and water-quenched HPDC specimens was 10.05, 12.85, and 8.94 μm, respectively. The average SDAS value of the as-cast GDC, furnace-cooled GDC, and water-quenched GDC specimens was 51.15, 55.6, and 47.15 μm, respectively (**Table 2**). The average SDAS value of all the GDC specimens was greater than that of the HPDC specimens (**Figure 2**).

Table 2: The average of secondary dendrite arm spacing

	as-cast	Furnace cooled	Water quenched
HPDC	10.05 ±0.56 μm	12.81 ±1.49 μm	8.94 ±1.23 μm
GDC	51.15 ±2.19 μm	55.61 ±2.61 μm	47.15 ±2.24 μm

As shown in **Table 2**, the average SDAS value of as-cast HPDC specimen was 10.05 μm, the average SDAS value of the furnace-cooled HPDC specimen was 12.85 μm, and the average SDAS value of the water-quenched HPDC specimen was 8.94 μm. **Table 2** shows that the average SDAS value of the as-cast GDC specimen was 51.15 μm, the furnace-cooled GDC specimen was 55.6 μm, and the average SDAS value of 47.15 μm was measured in the water-quenched GDC specimen. Through **Table 2**, the average SDAS value of all GDC specimens is greater than the average SDAS of all HPDC specimens.

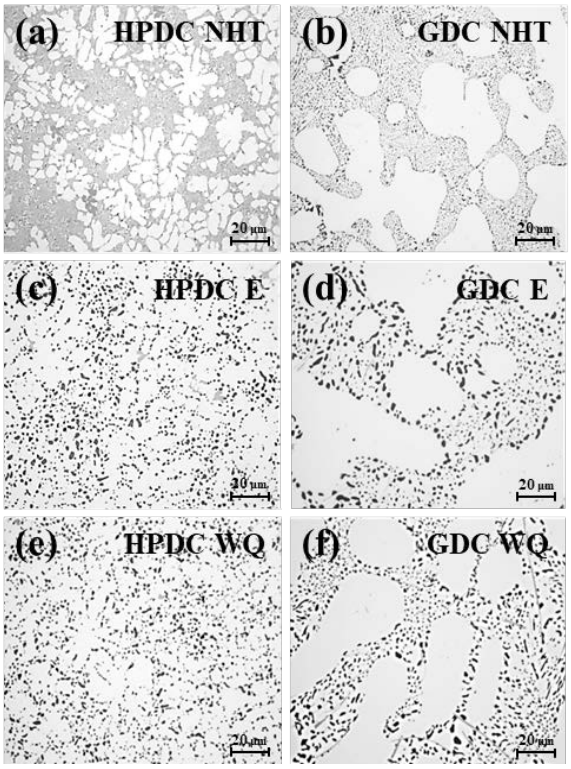

Figure 1: OM image showing microstructure of AA365 (a) as-cast HPDC; (b) as-cast GDC; (c) furnace-cooled HPDC; (d) furnace-cooled GDC; (e) water-quenched HPDC; (f) water-quenched GDC

As mentioned in the Experimental section, the casting process was varied when manufacturing the specimens to determine the effect of the grain size on the residual stress by using samples with different initial grain sizes. As shown in **Figure 2**, the specimens manufactured using HPDC had significantly smaller grain sizes than those manufactured using GDC. The cooling rate of HPDC is generally very high, from 50 to 125 K/s, which directly affects the size of the microstructural components, and in most cases, does not induce grain refinement during the HPDC aluminum casting process. HPDC is a process of filling molten metal into a mold at high speed and pressure. The production cycle is very short compared to that of other casting processes, making it highly productive. It was possible to precisely cast a product with a thin and complex shape, and the grains were fine because of the fast cooling speed **[21]-[22]**.

Table 3 presents the grain sizes of the specimens. The average grain size of the as-cast HPDC specimen without heat treatment was 13.17 μm, and the average grain size of the as-cast GDC

specimen was 448.39 μm, which is a 30-fold difference. The average grain size of the furnace-cooled HPDC and furnace-cooled GDC specimens was 13.66 and 653.81 μm, respectively. The average grain size of the water-quenched GDC and water-quenched HPDC specimens was 123.85 and 12.21 μm, respectively, where the average grain size of the water-quenched GDC specimen was about 10 times larger. The grain size of the HPDC specimen with the fine microstructure was smaller than that of the GDC specimen.

Table 3: The average grain size of HPDC, GDC

	as-cast	Furnace cooled	Water quenched
HPDC	13.17 μm	13.66 μm	12.21 μm
GDC	448.39 μm	653.81 μm	123.85 μm

Table 4: The value of residual stress of HPDC, GDC

	as-cast	Furnace cooled	Water quenched
HPDC	35±6 MPa	42±8 MPa	-56±6 MPa
GDC	57±5 MPa	89±12 MPa	-67±8 MPa

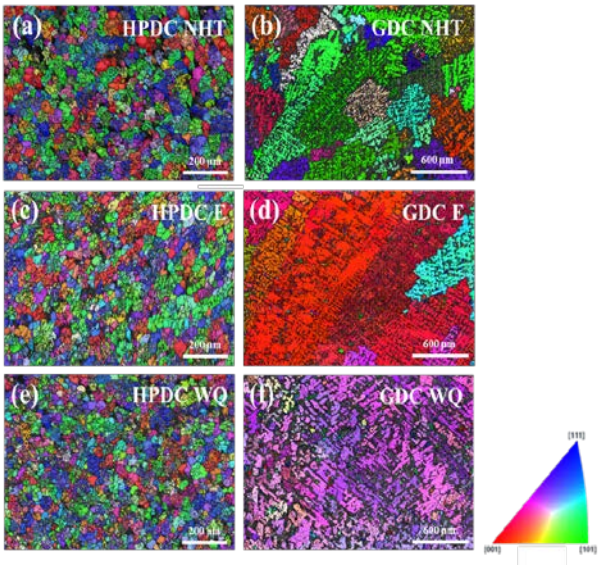

Figure 2: Inverse pole figure (IPF) notation for (a) as-cast HPDC; (b) as-cast GDC; (c) furnace-cooled HPDC; (d) furnace-cooled GDC; (e) water-quenched HPDC; (f) water-quenched GDC

3.2 Residual stress

X-ray diffraction (XRD) was used to measure the residual stress of the polycrystalline materials using a non-destructive method. The residual stress of the specimens was measured using an analyzer **[23]**. The residual stress in the as-cast GDC specimen was 57 MPa and that of the HPDC specimen was 35 MPa. The residual stress in the as-cast GDC specimen is approximately 20 MPa higher than that in the as-cast HPDC specimen. The residual stress in the furnace-cooled GDC specimen was 89 MPa and that in the furnace-cooled HPDC specimen was 42 MPa. The residual tensile stress of the furnace-cooled GDC specimen was almost twice as high. Owing to the fast cooling rate, the compressive residual stress was measured in the quenching water. The residual stress of the water-quenched HPDC specimen was ~56 MPa, and a compressive residual stress of ~67 MPa was measured for the water-quenched GGDC specimen, resulting in a difference of ~ 10 MPa between the stress of the two specimens. Overall, the residual stress of the GDC specimens exceeded that of the HPDC specimens.

As shown in **Tables 3** and **4**, the residual stress of the GDC specimen with a much larger grain size was greater than that of the HPDC specimen. The average grain size of the furnace-cooled specimen was approximately 50 times different, and the residual stress was also the largest. The grain size of the water-quenched specimen was approximately 10 times higher. The residual stress was also higher in the GDC specimen having a larger grain size. The initial grain size of the as-cast specimen without heat treatment was approximately 30 times higher. The residual stress of the as-cast GDC specimen with a large grain size was also larger.

Table 5: Fraction of high-angle grain boundary (> 15 °)

	as-cast	Furnace cooled	Water quenched
HPDC	94.78 %	93.2 %	94.92 %
GDC	87.1 %	88.6 %	84.59 %

Table 6: The average grain misorientation (GAM)

	as-cast	Furnace cooled	Water quenched
HPDC	16.41 °	19.15 °	17.96 °
GDC	12.19 °	13.98 °	13.99 °

3.4 Grain boundary

To determine why the residual stress varied according to the grain size, the grain boundaries and misorientations were first examined. As shown in **Tables 5** and **6**, the larger the grain size in the as-cast specimen, the smaller the high-angle grain boundary (HAGB) fraction and the smaller the average misorientation value. Similarly, in the furnace-cooled and water-quenched specimens, the smaller the grain size, the higher the high-angle grain boundary fraction and the higher the average misorientation

value. The larger the grain size, the lower the high-angle grain boundary (HAGB) fraction and the smaller the average misorientation value. The smaller the grain size, the higher the HAGB fraction and the larger the average misorientation.

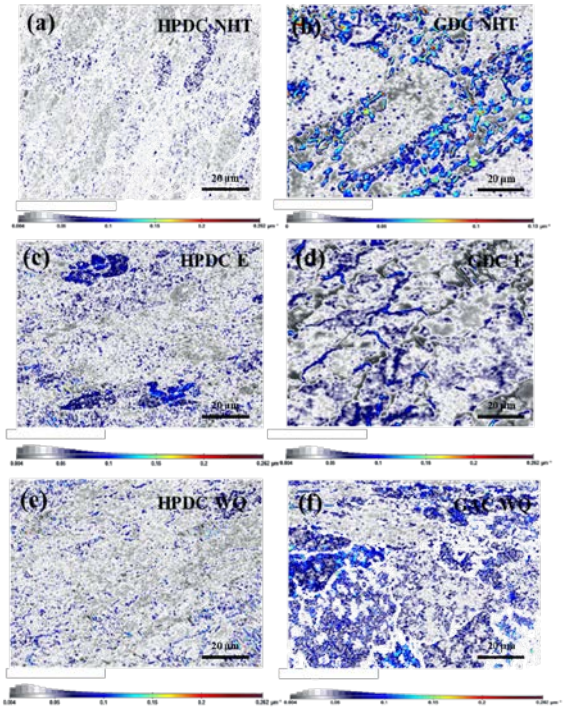

Figure 3: Geometrically necessary dislocation density (GND) of HPDC and GDC; (a) as-cast HPDC; (b) as-cast GDC; (c) furnace-cooled HPDC; (d) furnace-cooled GDC; (e) water-quenched HPDC; (f) water-quenched GDC

3.5 Dislocation density

As shown in **Figure 3**, more dislocations were distributed inside and around the grains of the GDC specimen than in the HPDC specimen. A large number of dislocations was distributed inside and around the grain. A larger distribution of low-angle grain boundaries (LAGBs) was present in the GDC specimens with large grain sizes (**Table 5**). Low-angle grain boundaries are less resistant to dislocations and are easily penetrated by dislocation **[24]**. Therefore, the larger the grain size, the greater the distribution of LAGBs; thus, the potential is distributed more widely inside and around the grains. During casting, faster cooling during metal solidification may reduce the accumulation of dislocations **[25]**. Large amounts of LAGBs were formed in the coarse grains, whereas the fraction of LAGBs in the fine grains was significantly lower.

The LAGBs have a lower resistance to potential movement than the HAGBs; therefore, they are easily penetrated by dislocations. The accumulated dislocations produce high stress concentrations and act as a potential site for microcrack initiation **[26]-[29]**.

4. Conclusion

$AlSi_{10}MnMg$ alloys with different initial grain sizes were prepared by high-pressure die casting and gravity die casting. The $AlSi_{10}MnMg$ alloys were heat treated at 500 °C for 2 h, then furnace-cooled and water-quenched to control the variables that may affect the residual stress or induce microstructural changes. The changes in the residual stress were analyzed according to the grain size. The average grain size of the as-cast HPDC specimen without heat treatment was approximately 30 times smaller than that of the as-cast GDC specimen, and the residual stress of the gravity mold-cast specimen with a large grain size was approximately 20 MPa. The grain size of the furnace-cooled GDC specimen was approximately 50 times larger than that of the furnace-cooled HPDC specimen, and the residual stress was approximately 40 MPa, showing the largest difference. The average grain sizes of the water-quenched GDC and HPDC specimens differed by ~10-fold, and the residual stress of the water-quenched GDC specimen was approximately 8 MPa higher. The larger the grain size, the more easily the low-angle grain boundaries are penetrated by dislocations. Therefore, the larger the grain size, the larger the distribution of low-angle grain boundaries. Thus, numerous dislocations are distributed inside and around the grain. This accumulated dislocation generates internal stress, resulting in stress concentration.

Acknowledgement

This work was conducted with the support of the Korea Basic Science Institute (National research Facilities and Equipment Center) grant funded by Ministry of Education (grant No. 2022R1A6C101B738).

Author Contributions

Conceptualization, M. Jeon and E. Lee; Methodology, M. Jeon; Software, M. Jeon; Validation, M. Jeon and E. Lee; Formal Analysis, M. Jeon; Investigation, M. Jeon; Resources M. Jeon; Data Curation, M. Jeon; Writing—Original Draft Preparation, M. Jeon; Writing—Review & Editing, E. Lee; Visualization, M. Jeon; Supervision, E. Lee; Project Administration, E. Lee; Funding Acquisition, E. Lee.

References

[1] P. D. Srivyas and M. S. Charoo, “Application of hybrid aluminum matrix composite in automotive industry,” Materials Today: Proceedings, vol. 18, part 7, pp. 3189-3200, 2019.

[2] S. B. Kim, Y. H. Cho, M. S. Jo, and J. M. Lee, “Optimization of solid solution treatment process for a high pressure die casting al-10si-0.3 mg-0.6 mn alloy to avoid blistering and improve the strength of the alloy,” Journal of Korea Foundry Society, vol. 40, no. 3, pp. 66-75, 2020.

[3] M. Nikawa, D. Sasai, Y. Mizutani, and M. Yamashita, “Evaluation of residual stress in die castings of Al-Si-Cu alloy considering material composition change in thickness direction,” International Journal of Automation Technology, vol. 15, no. 3, pp. 359-365, 2021.

[4] E. Lee, C. Walde, and B. Mishra, “Effects of cooling rate on precipitate evolution and residual stresses in Al–Si–Mn–Mg casting alloy,” Metals and Materials International, vol. 24, pp. 815-820, 2018.

[5] G. S. Schajer and P. S. Whitehead, “Hole-drilling method for measuring residual stresses,” Synthesis SEM Lectures on Experimental Mechanics, pp. 14-17, 2018.

[6] H. Farhangi, S. Norouzi, and M. Nili-Ahmadabadi, “Effects of casting process variables on the residual stress in Ni-base superalloys,” Journal of Materials Processing Technology, vol. 153-154, pp. 209-212, 2004.

[7] M. Wang, B. Song, Q. Wei, Y. Zhang, Y. Shi, “Effects of annealing on the microstructure and mechanical properties of selective laser melted AlSi7Mg alloy,” Materials Science and Engineering: A, vol. 739, pp. 463-472, 2019.

[8] S. S. Mohamed, A. M. Samuel, H. W. Doty, S. Valtierra, and F. H. Samuel, “Generation and relaxation of residual stresses in automotive cylinder blocks,” Advanced Applications of Hydrogen and Engineering Systems in the Automotive Industry, p. 77, 2020.

[9] T. W. Park, K. J. Kim, C. P. Han, Y. S. Lee, and J. H. Lim, “Deformation and residual stress of automotive frame by welding,” Transactions of the Korean Society of Automotive Engineers, vol. 19, no. 5, pp. 113-117, 2011.

[10] D. Sediako, J. Stroh, and S. Kianfar, “Residual stress in automotive powertrains: Methods and Analyses,” Materials Science Forum, vol. 1016, pp. 1291-1298, 2021.

[11] A. Tabatabaeian, A. R. Ghasemi, M. M. Shokrieh, B. Marzbanrad, M. Baraheni, and M. Fotouhi, “Residual stress in engineering materials: a review,” Advanced Engineering Materials, vol. 24, no. 3, 2021.

[12] D. H. Ko, B. M. Kim, T. J. Kim, H. J. Lim, and J. M. Lee, “FE-simulation and measurement of the residual stress in Al6061 during T6 heat treatment,” Transactions of the Korean Society of Mechanical Engineers, vol. A35, no. 7, pp. 717-722, 2011.

[13] N. Grillia, D. Hua, D. Yushub, F. Chena, and W. Yana, “Crystal plasticity model of residual stress in additive manufacturing,” arXiv preprint arXiv:2105.13257, 2021.

[14] Q. Wang, X. Leng, T. Yang, and J. Yan, “Effects of Fe—Al intermetallic compounds on interfacial bonding of clad materials,” Transactions of Nonferrous Metals Society of China, vol. 24, no. 1, pp. 279-284, 2014.

[15] R. Tian, C. Hang, Y. Tian, B. Wu, Y. Liu, and J. Zhao, “Interfacial Intermetallic Compound Growth in Sn-3ag-0.5 Cu/Cu Solder Joints Induced by Stress Gradient at Cryogenic Temperatures,” Journal of Alloys and Compounds, vol. 800, pp. 180-190, 2019.

[16] A. Niklas, A. Bakedano, S. Orden, M. da Silva, E. Nogués, and A. I. Fernández-Calvo, “Effect of microstructure and casting defects on the mechanical properties of secondary AlSi10MnMg (Fe) test parts manufactured by vacuum assisted high pressure die casting technology,” Materials Today: Proceedings, vol. 2, no. 10, part A, pp. 4931-4938, 2015.

[17] C. Gu, Y. Lu, E. Cinkilic, J. Miao, A. Klarner, X. Yan, and A. A. Luo, “Predicting grain structure in high pressure die casting of aluminum alloys: A coupled cellular automaton and process model,” Computational Materials Science, vol. 161, pp. 64-75, 2019.

[18] V. A. N. Righetti, T. M. B. Campos, L. B. Robatto, R. R. Rego, and G. P. Thim, “Non-destructive surface residual stress profiling by multireflection grazing incidence X-ray diffraction: A 7050 Al alloy study,” Experimental Mechanics, vol. 60, pp. 475-480, 2020.

[19] C. E. Murray and I. Cevdet Noyan, “Applied and residual stress determination using X-ray diffraction,” Practical Residual Stress Measurement Methods, pp. 139-161, 2013.

[20] C. Gawert and R. Bähr, “Automatic Determination of - 60 - Secondary Dendrite Arm Spacing in AlSi-Cast Microstructures,” Materials, vol. 14, no. 11, p. 2827, 2021.

[21] M. Žbontar, M. Petrič, and P. Mrvar, “The influence of cooling rate on microstructure and mechanical properties of AlSi9Cu3,” Metals, vol. 11, no. 2, p. 186, 2021.

[22] M. G. Kang, H. S. Yoon, C. U. Lee, T. S. Lim, S. J. Kim, and K. M. Yoon, “Development of pipe-inserted aluminum component by high pressure die-casting,” Transactions of the Korean Society of Automotive Engineers, vol. 30, no. 1, pp. 45-50, 2022.

[23] B. Kämpfe, “Investigation of residual stresses in microsystems using X-ray diffraction,” Materials Science and Engineering: A, vol. 288, no. 2, pp. 119-125, 2000.

[24] S. Chen and Q. Yu, “The role of low angle grain boundary in deformation of titanium and its size effect,” Scripta Materialia, vol. 163, pp. 148-151, 2019.

[25] T. Le, Q. Wei, J. Wang, P. Jin, M. Chen, and J. Ma, “Effect of different casting techniques on the microstructure and mechanical properties of AE44-2 magnesium alloy,” Materials Research Express, vol. 7, no. 11, 2020.

[26] R. Liu, Z. Liang, L. Lin, and M. Huang, “Dislocation source and pile-up in a twinning-induced plasticity steel at high-cycle fatigue,” Acta Metallurgica Sinica (English Letters), vol. 34, pp. 169-173, 2021.

[27] Y. F. Wang, C. X. Huang, Q. He, F. J. Guo, M. S. Wang, L. Y. Song, and Y. T. Zhu, “Heterostructure induced dispersive shear bands in heterostructured Cu,” Heterostructured Materials: Jenny Stanford Publishing, pp. 239-250, 2021.

[28] A. Dehghan-Manshadi and P. D. Hodgson, “Dependency of recrystallization mechanism to the initial grain size,” Metallurgical and Materials Transactions A, vol. 39, pp. 2830-2840, 2008.

[29] D. Zhang, Q. Yang, K. Guan, B. Li, N. Wang, P. Qin, B. Jiang, C. Sun, X. Qin, Z. Tian, Z. Cao, and J. Meng, “A high-strength low-rare-earth-alloyed magnesium alloy via traditional hot-extrusion,” Journal of Alloys and Compounds, vol. 810, 2019.